Engineering Structures 43 (2012) 21–30

Contents lists available at SciVerse ScienceDirect

Engineering Structures

journal homepage: www.elsevier.com/locate/engstruct

Identification of Rational Functions using two-degree-of-freedom model by forced vibration method

Bochao Cao, Partha P. Sarkar *

Wind Simulation & Testing Laboratory, Department of Aerospace Engineering, Iowa State University, Ames, IA 50011, USA

ARTICLE INFO

Article history:
Received 20 January 2012
Revised 10 April 2012
Accepted 7 May 2012
Available online 12 June 2012

Keywords:
Rational Functions
Self-excited forces
Two-degree-of-freedom model
Forced vibration method
Streamlined section model
Rectangular section model

ABSTRACT

In prediction of self-excited forces and flutter instability of flexible structures, time domain method has distinct advantages. Rational Functions that are used to formulate self-excited aerodynamic forces in time domain were indirectly extracted from experimentally obtained flutter derivatives in the past. Recently, an algorithm was published to directly extract the Rational Functions from wind tunnel section model tests in free vibration. To overcome the limitations of free vibration technique, a new algorithm that is developed for direct extraction of the Rational Functions from section model tests using a forced vibration technique is presented here. The new algorithm can be used to extract all the Rational Functions associated with one, two or three degree-of-freedom motion (vertical, lateral and torsional) of a section model. To validate the new algorithm, forced vibration wind tunnel tests in two degrees of freedom (vertical and torsional) were performed on a streamlined bridge deck section model with width-to-depth ratio $B/D = 15{:}1$ and also a bluff rectangular section model with $B/D = 5{:}1$. This is a significant improvement from other forced vibration methods that require separate one-degree-of-freedom model tests which are dependent on phase angle difference between aerodynamic loads and displacements.

1. Introduction

In design of long-span bridges, it is important to identify whether there is aeroelastic instability (flutter) at wind speeds below the design wind speed. Scanlan and Tomko [1] developed a technique to carry out flutter analysis in frequency domain using experimentally obtained flutter derivatives. This laid the foundation for the development of various efficient methods to extract flutter derivatives from wind tunnel experiments, such as Scanlan [2] and Sarkar et al.'s [3] Modified Ibrahim Time Domain (MITD) method, Brownjohn and Jakobsen's [4] Covariance Block Hankel Matrix (CBHM) method, and Gan Chowdhury and Sarkar's [5] Iterative Least Squares (ILS) method, and many other methods. In recent years, time domain analysis (e.g., [6–10]) has been gaining popularity. In time domain analysis, the equations of motion are frequency independent so structural and aerodynamic nonlinearities can be incorporated. For time domain analysis, the self-excited forces acting on a flexible structure can be approximately represented by Rational Functions in Laplace domain. Roger [11] formulated the least squares Rational Function Approximation (LS-RFA) formulation, and Karpel [12] developed the minimum state Rational Function Approximation (MS-RFA) formulation. Using these RFA formulations, one can obtain Rational Function Coefficients from flutter derivatives by approximation techniques. RFA formulation has been applied to bridge aerodynamics by several researchers including Xie [13], Xiang et al. [14], Wilde et al. [15] and Chen et al. [16]. However, this is an indirect way to obtain Rational Function Coefficients since flutter derivatives need to be obtained first from experiments that need to be repeated for several wind speeds. Thus, to make the process of extracting the Rational Function Coefficients more efficient, Gan Chowdhury and Sarkar [17] developed a new method based on free vibration of section models where both displacements and surface pressures of the model were simultaneously recorded and used. It is known that the free vibration method has some limitations compared to the forced vibration method because it is particularly unsuitable for higher wind speeds, large amplitudes of motion, turbulent flow, aerodynamically unstable cross-sections and flow regimes where vortex-shedding dominates the excitation. This provided the motivation to develop a forced vibration experimental method to extract the Rational Functions. However, the current forced vibration techniques for extraction of flutter derivatives [18,19] or Rational Function Coefficients [20] have some limitations. Firstly, these techniques are based on the *phase difference* between simultaneously obtained displacement and aerodynamic load time histories. In a recently concluded comparative and sensitivity study [21], it was shown that in a phase-difference-dependent forced vibration technique to extract the four flutter derivatives based on a pure torsional motion system, the errors in A_2^* and H_2^*

* Corresponding author. Address: Wind Simulation and Testing Laboratory, Department of Aerospace Engineering, Iowa State University, 2271 Howe Hall, Room 1200, Ames, IA 50011-2271, USA. Tel.: +1 515 294 0719.
E-mail address: ppsarkar@iastate.edu (P.P. Sarkar).

0141-0296/$ - see front matter © 2012 Elsevier Ltd. All rights reserved.
http://dx.doi.org/10.1016/j.engstruct.2012.05.003

Nomenclature

$\hat{L}_{se}(t)$	aerodynamic self-excited lift in Laplace domain
$\hat{M}_{se}(t)$	aerodynamic self-excited moment in Laplace domain
ρ	air density
U	mean wind speed, m/s
B	width of the bridge deck
D	height of bridge deck
B/D	aspect ratio of bridge deck model
K	(=$B\omega/U$), reduced frequency of the vibration
p	(=iK), nondimensional Laplace domain variable
$\hat{h}$	vertical displacement in Laplace domain
$\hat{\alpha}$	torsional displacement in Laplace domain
$\underline{Q}$	matrix of Rational Functions
$\hat{q}$	displacement vector in Laplace domain
$\underline{A}_0$, $\underline{A}_1$, $\underline{F}$, λ	Rational Function Coefficients
$L_{se}(t)$	aerodynamic self-excited lift in time domain
$M_{se}(t)$	aerodynamic self-excited moment in time domain
$\underline{\psi}_1$, …, $\underline{\psi}_6$	vectors that include all the Rational Function Coefficients
$A_1^*,\ldots,A_4^*$	flutter derivatives per unit length, aerodynamic moment
$H_1^*,\ldots,H_4^*$	flutter derivatives per unit length, lift force
$h(t)$	vertical displacement in time domain
$\alpha(t)$	torsional displacement in time domain
τ	dummy time variable in the integration
ρ_{xy}	cross-correlation coefficient
err_{peak}	percentage peak error
x	experimentally obtained time history
y	simulated time history
$\hat{x}_i$	peak values of time history x
$\hat{y}_i$	peak values of time history y

could be significant, since slight errors in the phase difference obtained from the experiment gets amplified in the formulation that defines and H_2^*. Similar observation was made in the phase-difference-dependent technique to extract Rational Function Coefficients [20]. Secondly, earlier forced vibration techniques were all based on one degree-of-freedom (DOF) motion (vertical or torsional), and aeroelastic coefficients (flutter derivatives or Rational Function Coefficients) associated with two degrees of freedom were obtained by combining results from two separate one DOF tests. Considering there is a physical difference between the aerodynamics of one DOF and two DOF motions, there might be errors introduced in the aeroelastic coefficients obtained by one DOF system because the actual aerodynamic interaction of a two DOF system may not be captured well. Thus, in this paper, a forced vibration method that does not use the *phase difference* is described to extract all the Rational Function Coefficients simultaneously from a two-DOF dynamic system for the first time. Moreover, the method developed in this paper is more efficient than earlier ones, since it requires data obtained at two wind speeds only to solve for the full set of Rational Function Coefficients.

2. Formulation and algorithm

Using Minimum State Rational Function Approximation (MSRFA) formulation, Karpel [12] derived the following Laplace domain formulation of aerodynamic self-excited forces:

$$\begin{bmatrix}\hat{L}_{se}\\ \hat{M}_{se}\end{bmatrix} = \underline{V}_f \underline{Q} \hat{\underline{q}} = \begin{bmatrix}\frac{1}{2}\rho U^2 B & 0\\ 0 & \frac{1}{2}\rho U^2 B^2\end{bmatrix} \cdot \begin{bmatrix}(\underline{A}_0)_{11}+(\underline{A}_1)_{11}p+\frac{(\underline{F})_{11}p}{p+\lambda} & (\underline{A}_0)_{12}+(\underline{A}_1)_{12}p+\frac{(\underline{F})_{12}p}{p+\lambda}\\ (\underline{A}_0)_{21}+(\underline{A}_1)_{21}p+\frac{(\underline{F})_{21}p}{p+\lambda} & (\underline{A}_0)_{22}+(\underline{A}_1)_{22}p+\frac{(\underline{F})_{22}p}{p+\lambda}\end{bmatrix}\begin{bmatrix}\hat{h}/B\\ \hat{\alpha}\end{bmatrix} \tag{1}$$

where B = width of the bridge deck, U = mean wind velocity, $p = iK$ is nondimensional Laplace domain variable, $K = B\omega/U$ = reduced frequency of the vibration, where $\omega = 2\pi f$ = circular frequency of the vibration, '$\hat{}$' denotes the Laplace transformation of the corresponding time domain function, L_{se} and M_{se} are self-excited lift and moment, respectively, h is vertical displacement and α is torsional displacement. $\underline{Q}$ is Rational Function matrix consisting of four Rational Functions and $\underline{A}_0$, $\underline{A}_1$, $\underline{F}$and λ are Rational Function Coefficients. $\underline{A}_0$, $\underline{A}_1$ are stiffness matrix and damping matrix, respectively, and $\underline{F}$ is a lag matrix, all of order 2×2, λ is a lag coefficient, and $\hat{\underline{q}} = [\hat{h}/B\ \hat{\alpha}]^T$ is the displacement vector. Multiplying both sides with $p+\lambda$, and applying inverse Laplace transformation on both sides of Eq. (1), two time-domain equations for lift and moment can be obtained respectively as:

$$\dot{L}_{se} + \lambda_L \frac{U}{B} L_{se} = \frac{1}{2}\rho U^2 B\left(\left(\frac{U}{B}\right)\underline{\psi}_1\underline{q} + \underline{\psi}_2\dot{\underline{q}} + \left(\frac{B}{U}\right)\underline{\psi}_3\ddot{\underline{q}}\right) \tag{2}$$

$$\dot{M}_{se} + \lambda_M \frac{U}{B} M_{se} = \frac{1}{2}\rho U^2 B^2\left(\left(\frac{U}{B}\right)\underline{\psi}_4\underline{q} + \underline{\psi}_5\dot{\underline{q}} + \left(\frac{B}{U}\right)\underline{\psi}_6\ddot{\underline{q}}\right) \tag{3}$$

where

$$\underline{\psi}_1 = \left[\lambda_L(\underline{A}_0)_{11}\quad \lambda_L(\underline{A}_0)_{12}\right],$$
$$\underline{\psi}_2 = \left[(\underline{A}_0)_{11}+\lambda_L(\underline{A}_1)_{11}+(F)_{11}\quad (\underline{A}_0)_{12}+\lambda_L(\underline{A}_1)_{12}+(F)_{12}\right],$$
$$\underline{\psi}_3 = \left[(\underline{A}_1)_{11}\quad (\underline{A}_1)_{12}\right],\quad \underline{\psi}_4 = \left[\lambda_M(\underline{A}_0)_{21}\quad \lambda_M(\underline{A}_0)_{22}\right],$$
$$\underline{\psi}_5 = \left[(\underline{A}_0)_{21}+\lambda_M(\underline{A}_1)_{21}+(\underline{F})_{21}\quad (\underline{A}_0)_{22}+\lambda_M(\underline{A}_1)_{22}+(\underline{F})_{22}\right],$$
$$\underline{\psi}_6 = \left[(\underline{A}_1)_{21}\quad (\underline{A}_1)_{22}\right].$$

Eqs. (1)–(3) are slightly modified forms of those mentioned in [17]. Eqs. (2) and (3) can be rewritten in matrix form as:

$$\left[\underline{\psi}_1\quad \underline{\psi}_2\quad \underline{\psi}_3\quad -\lambda_L\right]\begin{bmatrix}\frac{1}{2}\rho U^2 B(\frac{U}{B})\underline{q}\\ \frac{1}{2}\rho U^2 B\dot{\underline{q}}\\ \frac{1}{2}\rho U^2 B(\frac{B}{U})\ddot{\underline{q}}\\ \frac{U}{B}\underline{L}_{se}\end{bmatrix} = \dot{\underline{L}}_{se} \tag{4}$$

$$\left[\underline{\psi}_4\quad \underline{\psi}_5\quad \underline{\psi}_6\quad -\lambda_M\right]\begin{bmatrix}\frac{1}{2}\rho U^2 B^2(\frac{U}{B})\underline{q}\\ \frac{1}{2}\rho U^2 B^2\dot{\underline{q}}\\ \frac{1}{2}\rho U^2 B^2(\frac{B}{U})\ddot{\underline{q}}\\ \frac{U}{B}\underline{M}_{se}\end{bmatrix} = \dot{\underline{M}}_{se} \tag{5}$$

Let

$$\underline{A}_L = \left[\underline{\psi}_1\quad \underline{\psi}_2\quad \underline{\psi}_3\quad -\lambda_L\right],\quad \underline{X}_L = \begin{bmatrix}\frac{1}{2}\rho U^2 B(\frac{U}{B})\underline{q}\\ \frac{1}{2}\rho U^2 B\dot{\underline{q}}\\ \frac{1}{2}\rho U^2 B(\frac{B}{U})\ddot{\underline{q}}\\ \frac{U}{B}\underline{L}_{se}\end{bmatrix},\quad \underline{b}_L = \dot{\underline{L}}_{se},$$

$$\underline{A_M} = \begin{bmatrix} \underline{\psi_4} & \underline{\psi_5} & \underline{\psi_6} & -\lambda_M \end{bmatrix}, \quad \underline{X_M} = \begin{bmatrix} \frac{1}{2}\rho U^2 B^2 (\frac{U}{B})\underline{q} \\ \frac{1}{2}\rho U^2 B^2 \underline{\dot{q}} \\ \frac{1}{2}\rho U^2 B^2 (\frac{B}{U})\underline{\ddot{q}} \\ \frac{U}{B}\underline{M_{se}} \end{bmatrix}, \quad \underline{b_M} = \underline{\dot{M}_{se}}.$$

Thus,

$$\underline{A_L X_L} = \underline{\dot{L}_{se}}, \quad \underline{A_M X_M} = \underline{\dot{M}_{se}} \tag{6}$$

It can be seen that all the Rational Function Coefficients that need to be identified are included in $\underline{A_L}$ and $\underline{A_M}$. Therefore, the problem reduces to extracting $\underline{A_L}$ and $\underline{A_M}$ from a two-DOF test. In a forced vibration experiment, displacement and aeroelastic force time histories are recorded, and their derivatives can be obtained by finite difference method applied to original time histories. Thus, vectors $\underline{X_L}$, $\underline{X_M}$, $\underline{b_L}$ and $\underline{b_M}$ in the above equations can be formulated. Finally, vectors $\underline{A_L}$ and $\underline{A_M}$ can be solved by Least Squares method as:

$$\underline{A_L} = (\underline{b_L X_L^T})(\underline{X_L X_L^T})^{-1}, \quad \underline{A_M} = (\underline{b_M X_M^T})(\underline{X_M X_M^T})^{-1} \tag{7}$$

3. Experimental set-up

3.1. Description of wind tunnel used

The experiments were performed in the Bill James Open-Return Wind Tunnel, which is located in the Wind Simulation and Testing Laboratory (WiST Lab) in the Department of Aerospace Engineering at Iowa State University. This wind tunnel has a test section of 0.915 m (3.0 ft) width by 0.762 m (2.5 ft) height and its maximum wind velocity is 75 m/s (246 ft/s).

3.2. Model, suspension system and forced vibration mechanism

To validate the method stated in this paper, experiments were carried out on both a streamlined model and a bluff model. The streamlined bridge deck section model was used in both one-DOF experiment and two-DOF experiment as shown in Figs. 1 and 2 (see also [22]). The streamlined model is composed of a shallow box girder section and two semi-circular fairings at the edges. The length, chord length and thickness of the model are about 0.533 m, 0.3 m, and 0.02 m, respectively. The bluff section model is rectangular with a width-to-depth ratio (B/D) of 5:1, and the length, chord length and thickness of the model are about 0.533 m, 0.16 m, and 0.032 m, respectively (see also [21]). To reduce the edge effects, two plexiglass end plates were used on both models as seen in Fig. 2.

The three-DOF model suspension system used in this experiment is shown in Fig. 2. This system, developed by Sarkar et al. [23], enables vertical, horizontal and torsional motions of the model. To realize forced sinusoidal motions of the section model with constant amplitude and frequency in the experiments, a driving mechanism (Fig. 3) was used. The driving mechanism is placed above the test section. It consists of two motors, which are used to drive vertical and torsional motions of the model, respectively. The section model is driven by four aluminum rods which are connected with the driving mechanism, as seen in Fig. 2. Thus, vertical, torsional, or combined vertical-torsional two-DOF sinusoidal motion of the section model can be generated using this driving mechanism. Moreover, by changing the rotating speed of two motors using two separate controllers, the two frequencies of model vibration in two degrees of freedom can be changed independently.

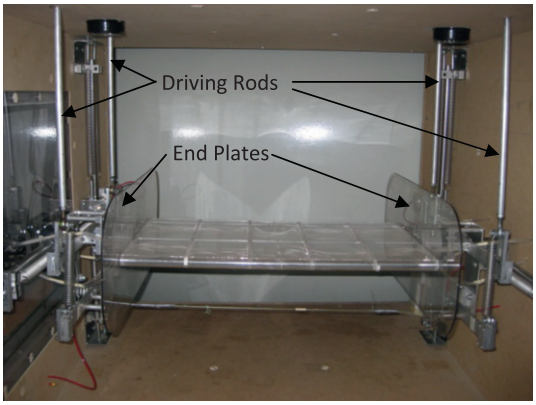

Fig. 2. Model and suspension system.

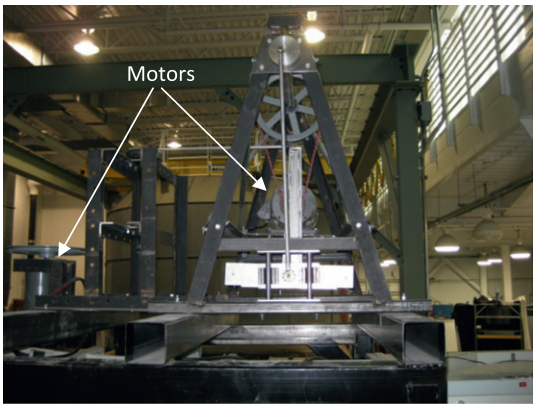

Fig. 3. Driving mechanism.

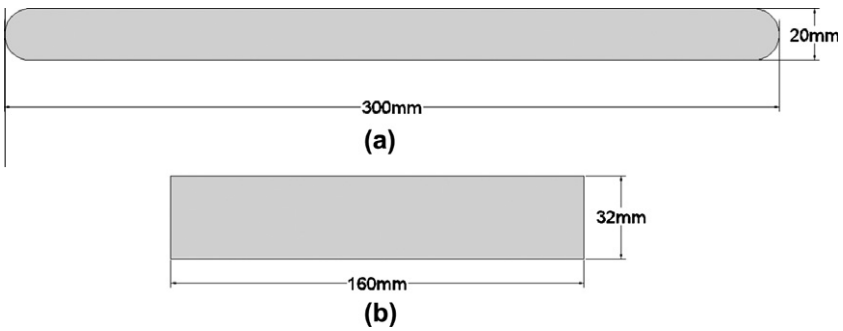

Fig. 1. Cross-section of models used in the experiments: (a) streamlined and (b) bluff.

3.3. Displacement measurement

The vertical displacement of the model was measured by measuring the elastic force in each of two springs which is connected to the model at one end and a strain gage force transducer at the other end. The torsional displacement was measured by measuring the torque at one end of the model shaft using a torque transducer which is mounted on the suspension system. LabVIEW was used for data acquisition, where the sampling rate was set at 625 Hz.

3.4. Aeroelastic force measurement

The algorithm stated in this paper requires time histories of aeroelastic forces acting on the model while it vibrates, in addition to the displacement time histories of the model. Therefore, surface pressures were measured on the model through a row of pressure taps located on the upper and lower surfaces of the model along the mid-plane for both streamlined and bluff models. In total, 42 pressure taps for streamlined model and 32 pressure taps for bluff model were used in the test. The pressure taps are equally distributed on the top and bottom surfaces and they are denser on the upstream side than the downstream side of the models. Two 64-channel pressure modules (Scanivalve ZOC33/64 Px) were used to measure the pressure. The sampling rate for pressure measurement was 312.5 Hz (half of displacement sampling rate) in the experiment. To synchronize the pressure data with the displacement data, the pressure transducers were set to work in external-trigger mode. LabVIEW (National Instrument) was used for displacement data acquisition and a separate program RAD (Scanivalve) was used to collect the pressure data. LabVIEW was programmed to output a digital signal when the displacement data acquisition started so that the pressure data acquisition system would get externally triggered to synchronously start the pressure data acquisition. The total sampling time was set as 10 seconds for all the tests.

4. Numerical tests

4.1. Numerical simulation and noise test

Before conducting the wind tunnel tests, numerical tests were carried out first to confirm that the algorithm developed here works well in extracting Rational Function Coefficients of bridge decks with both streamlined and bluff cross-sections. In the numerical tests, flutter derivatives of a bluff rectangular (B/D = 5:1) section model as extracted in [19] were used to generate lift and moment time histories at two wind speeds with given vertical and torsional displacement time histories as sinusoidal functions. The generated lift and moment were substituted in the algorithm to extract Rational Function Coefficients for the model, and the Rational Function matrix which contains four Rational Functions was computed using following formulation:

$$\underline{Q} = \begin{bmatrix} (\underline{A}_0)_{11} + (\underline{A}_1)_{11}p + \frac{(\underline{F})_{11}p}{p+\lambda} & (\underline{A}_0)_{12} + (\underline{A}_1)_{12}p + \frac{(\underline{F})_{12}p}{p+\lambda} \\ (\underline{A}_0)_{21} + (\underline{A}_1)_{21}p + \frac{(\underline{F})_{21}p}{p+\lambda} & (\underline{A}_0)_{22} + (\underline{A}_1)_{22}p + \frac{(\underline{F})_{22}p}{p+\lambda} \end{bmatrix} \tag{8}$$

To assess the accuracy of the extracted Rational Functions, they were converted to flutter derivatives using following relationships:

$$\begin{aligned} H_1^* &= imag(\underline{Q}_{11})/K^2, \quad H_4^* = real(\underline{Q}_{11})/K^2, \\ A_1^* &= imag(\underline{Q}_{21})/K^2, \quad A_4^* = real(\underline{Q}_{21})/K^2 \\ H_2^* &= imag(\underline{Q}_{12})/K^2, \quad H_3^* = real(\underline{Q}_{12})/K^2, \\ A_2^* &= imag(\underline{Q}_{22})/K^2, \quad A_3^* = real(\underline{Q}_{22})/K^2 \end{aligned} \tag{9}$$

The obtained flutter derivatives (referred RFA) were compared with the original ones used at the beginning of the simulation as shown in Fig. 4. As can be seen in the plots, all eight flutter derivatives compare very well with the original ones, which proves that the Rational Function formulation with only one lag term as used here is accurate enough to approximate flutter derivatives of a bluff rectangular cross-section model, even at high reduced velocities where some flutter derivatives could have complex trends. Moreover, this comparison shows that the algorithm developed here can work very well in extracting Rational Function Coefficients from forced vibration experimental data. To quantitatively assess the error in the obtained Rational Function Coefficients, they were converted to flutter derivatives at exact reduced velocities where original experimental data in [19] were obtained and the error function as given by Eq. (10) was calculated to evaluate the percentage error:

$$err = \frac{\sum_{j=1}^{8}\left[\sqrt{\sum_{i=1}^{N}\left(X_i^{(j)} - X_i^{0(j)}\right)^2}\Big/\sqrt{\sum_{i=1}^{N}\left(X_i^{0(j)}\right)^2}\right]}{8} \times 100\% \tag{10}$$

where $X_i^{(j)}$ is the jth flutter derivative of the model calculated from Rational Functions and evaluated at the ith reduced velocity point, and X(1)–X(8) correspond to H_1^*–H_4^* and A_1^*–A_4^*, respectively, and $X_i^{0(j)}$ is the corresponding original flutter derivative value given in [19], and N is the number of the reduced velocity points involved in the calculation. Using this error function, the percentage error was calculated as 8.14% which is acceptable considering data at only two wind velocities were used in the simulation to extract all the Rational Function Coefficients and the accuracy will certainly be improved by introducing data from more number of wind velocities.

Some noise tests were performed to test the robustness of the algorithm. White noise with different standard deviations was added to the numerically generated displacement and corresponding load (lift, moment) time histories obtained by using the original flutter derivatives given in [19]. The standard deviation of the noise was chosen as certain percentage (2%, 5% and 10%) of time history amplitudes of displacements (h, α) and loads. The flutter derivatives from the obtained Rational Functions from the noisy data were compared with ones extracted from the numerically generated time histories without any noise, and the errors were computed using Eq. (10), except the $X_i^{0(j)}$ here is the flutter derivative obtained from noise-free time histories and the $X_i^{(j)}$ is obtained from contaminated ones. The results are listed in Table 1 which shows a percentage error below 10% even with a 10% noise. Thus, the algorithm is reasonably robust.

4.2. Effect of time step on accuracy of the algorithm

In the algorithm, the displacement time histories need to be numerically differentiated twice to get acceleration time histories and also the first derivatives of the load time histories need to be evaluated using numerical method. Thus, the time step chosen in the finite difference method to calculate numerical derivatives could affect the accuracy of the extracted coefficients, especially when noise is present in the data. In current research, second order central difference method was used to evaluate derivatives. To investigate the consistency of the algorithm with different time steps chosen, numerical tests were carried out with larger time steps and also with 5% noise added to the displacement and load time histories.

The time step in the original numerical test was set as 0.0032 s which coincides with the experimental sampling period, and the ones used in current test were 0.005 s and 0.01 s which are about twice and three times of the original one. The coefficients extracted from 5% noise contaminated time histories and with two larger time steps were compared with ones extracted from clean time histories and with original time step. The errors were calculated using Eq. (10) as in the noise tests. It turns out that the percentage error for time step of 0.005 s is 4.18% and that for time step of 0.01 s is 6.54% which are both acceptable, although time steps are about two to three times the original time step of 0.0032 s.

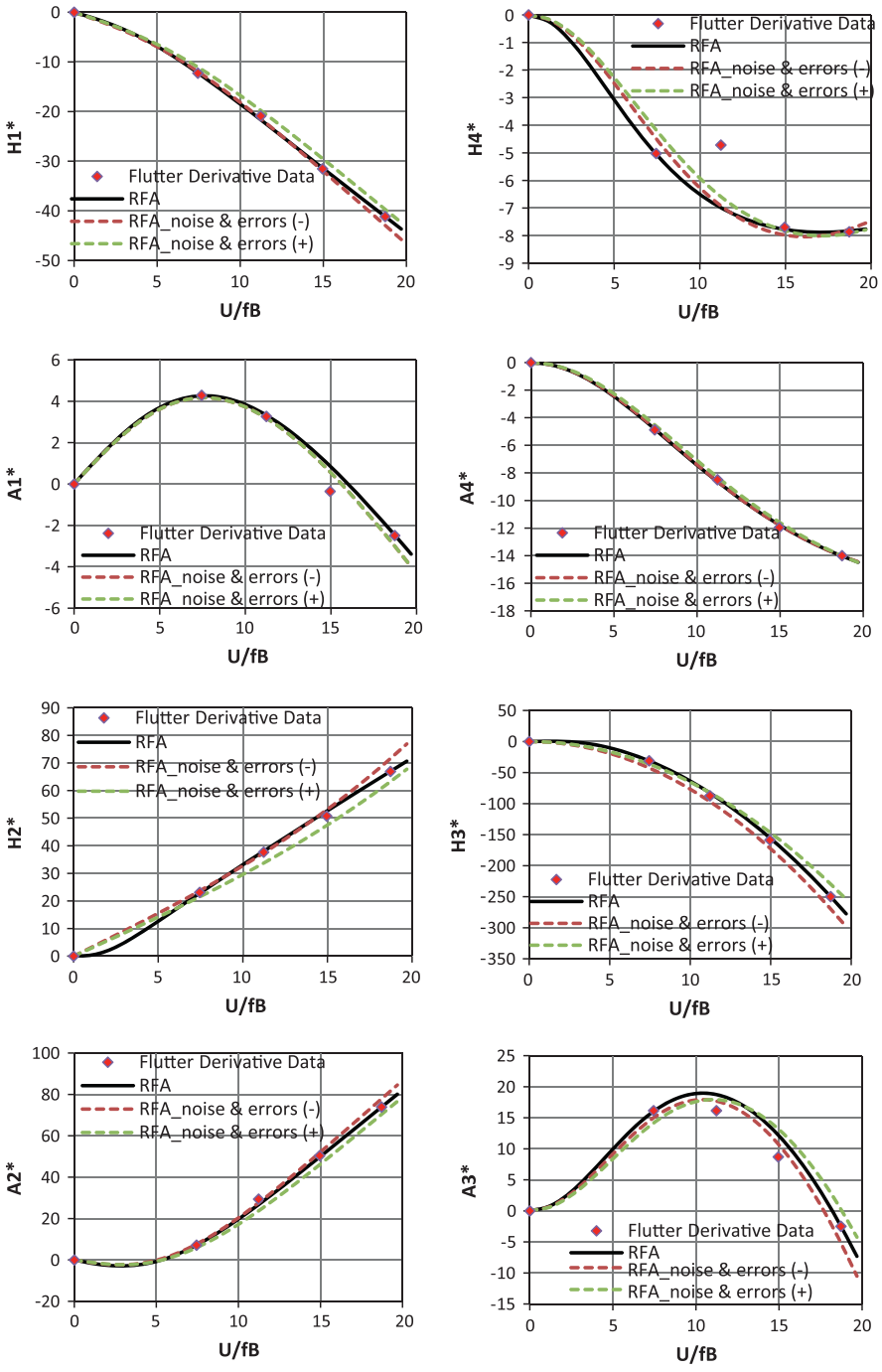

Fig. 4. Numerically extracted Ration Function Coefficients from clean time histories and the time histories contaminated by noises and with errors added.

Table 1
Percentage errors shown in noise tests.

2% Noise	5% Noise	10% Noise
Err (%) Eq. (10)		
1.74	3.92	9.39

4.3. Experimental error estimate and resulted error in the coefficients

In addition to electronic noise, errors could also be introduced into real experimental data either through equipment error or operational error from experimentalists. In this section, numerical tests were performed to confirm the algorithm could still work well when both noise and errors are present in the data.

For current algorithm, the input data are model displacements, h and α, aerodynamic loads, L and M, and the input parameters are wind velocity, U, and air density, ρ. In this numerical test, error was directly added to the specified parameters and the amplitudes for time history data.

In the experiment, the model displacements were obtained by measuring spring forces as mentioned earlier under experimental set-up and thus errors could be introduced from the error in the force transducers and the calibration of transducers. Moreover, considering that angle measurement could have more error than length measurement, 3% error is given to vertical displacement, h, while 5% error is given to torsional displacement, α. The errors in the aerodynamic loads could come from the pressure transducers, the pressure tubing, and the error from numerical method used

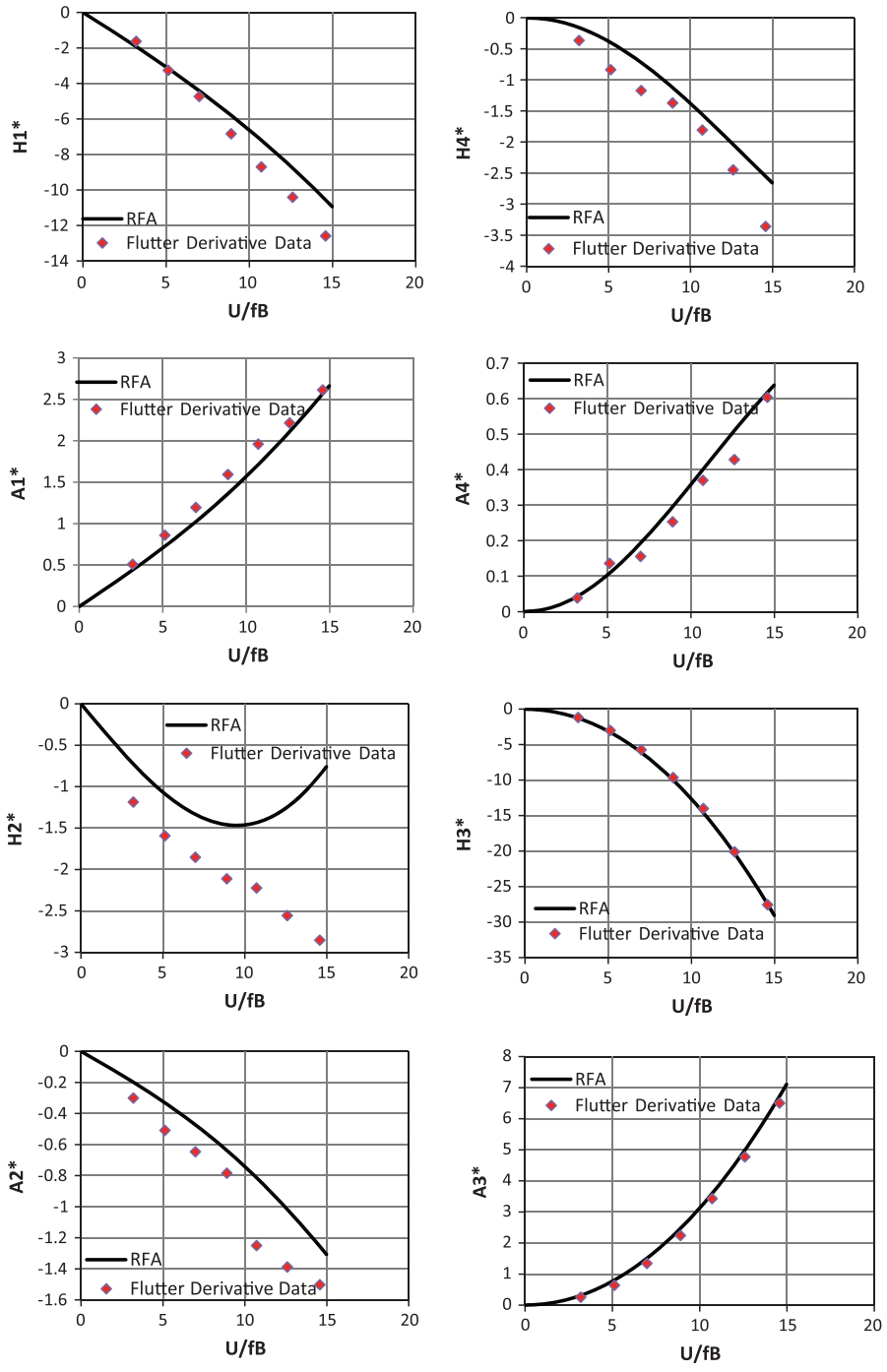

Fig. 5. Comparison of experimentally obtained flutter derivatives [17] and those from Rational Functions for the streamlined section model.

to integrate surface pressure into loads. Considering that integration of pressures to calculate moment could have more error than those from calculating lift, 3% error is assigned to lift, while 5% error is assigned to moment. The air density depends on the temperature and atmospheric pressure and does not change much, so only 1% error is assigned. Finally, the error in the wind velocity could come from the measurement of the dynamic pressure using Pitot tube and the error in the air density, thus 3% error is assigned. In the test, 5% noise and two combinations of errors, all positive or all negative, were given to simulate real experimental environment. The resulting flutter derivatives are plotted in Fig. 4 (referred RFA_noise and errors (±)) to compare with the results from clean data and the original flutter derivative data. It can be seen in the plots that the errors in the extracted aeroelastic parameters increase with reduced velocity, however, this occurs in a very small range. The errors were also quantified by error Eq. (10), which are 5.90% for the negative error case and 6.88% for the positive error case. Thus, even with estimated errors and noise added in the data, the algorithm can still be used to accurately extract all the coefficients.

5. Experimental results and discussion

For the streamlined bridge deck section model, wind tunnel tests were performed at five wind speeds: 2.8 m/s, 5.8 m/s, 8.6 m/s, 11.7 m/s, 14.4 m/s. The model was forced to move in

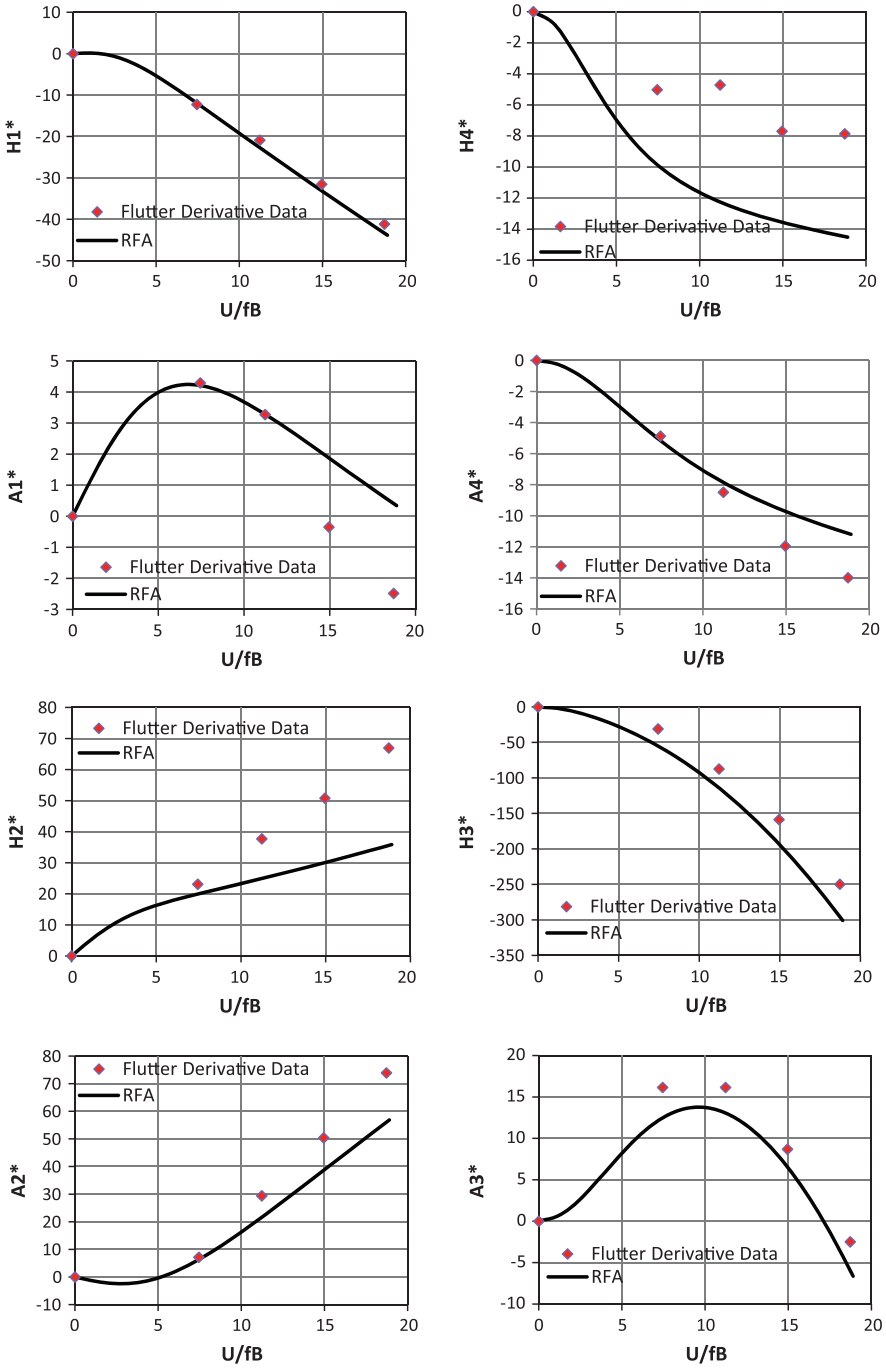

Fig. 6. Comparison of experimentally obtained flutter derivatives [19] and those from Rational Functions for the bluff section model.

two DOFs (vertical and torsional) at frequencies that were both around 2.5 Hz. Data obtained at two wind velocities, 2.8 m/s and 14.4 m/s, were used in the algorithm to solve for all the Rational Function Coefficients. The results are given below:

$$\underline{A}_0 = \begin{bmatrix} 0.3273 & -6.2384 \\ -0.0970 & 1.3818 \end{bmatrix}, \quad \underline{A}_1 = \begin{bmatrix} -3.7549 & -1.4947 \\ 0.8510 & -0.3819 \end{bmatrix},$$
$$\underline{F} = \begin{bmatrix} -0.9484 & 1.3397 \\ 0.2689 & -0.1682 \end{bmatrix}, \quad \lambda_L = 0.1843, \quad \lambda_M = 0.2239$$

For the bluff rectangular section model, experiments were carried out at wind speeds of 2.9 m/s, 5.9 m/s, 8.7 m/s, 11.6 m/s, 14.6 m/s. In these tests, the model was forced to vibrate in the same way and at same frequencies as what was set in the experiment of streamlined model. Data obtained at wind speeds of 5.9 m/s and 14.6 m/s were used in the algorithm to extract all the Rational Function Coefficients for this bluff section model, which are given below:

$$\underline{A}_0 = \begin{bmatrix} -0.0618 & -7.9085 \\ -0.0387 & -0.6258 \end{bmatrix}, \quad \underline{A}_1 = \begin{bmatrix} -0.7820 & 7.3997 \\ -1.7649 & -1.0621 \end{bmatrix},$$
$$\underline{F} = \begin{bmatrix} -10.4613 & -5.7309 \\ -1.5021 & 2.9637 \end{bmatrix}, \quad \lambda_L = 1.2048, \quad \lambda_M = 0.7091$$

To validate the obtained Rational Function Coefficients, they were converted to flutter derivatives using Eq. (9) as what was done in the numerical tests. The flutter derivatives computed using Rational Functions for the streamlined model were compared with

those directly extracted from a free vibration experiment carried out by Gan Chowdhury and Sarkar [17] on the same model and plotted in Fig. 5. While the flutter derivatives obtained from Rational Functions for the bluff rectangular model were compared with those directly extracted from a forced vibration experiment by Matsumoto [19] on a model with the same shape and same aspect ratio, $B/D = 5$. The flutter derivatives for the bluff model were plotted in Fig. 6.

It can be seen from Fig. 5 that, all flutter derivatives for the streamlined section model that are converted from Rational Functions match with directly extracted ones very well, except for H_2^*. In an earlier research by Cao and Sarkar [20] where the same streamlined model was discussed, similar phenomenon was observed and some numerical tests have been performed there on the flutter derivatives of this model. The tests showed that, for this model, H_2^* derivative is most sensitive to the error in the input time histories. Moreover, in that study, the H_2^* curve changed from the original shape to a shape similar to what was obtained here with just 7% error added to the time histories generated by the original flutter derivatives.

The comparison of flutter derivatives for the bluff section model, as shown in Fig. 6, is a little worse than that of the streamlined model, however the comparison of H_1^*, A_4^*, H_3^* and A_3^* is quite good, while the comparison of H_4^*, A_1^*, H_2^* and A_2^* is good for low reduced velocity region (less than 10) but slightly off at higher reduced velocities.

By directly applying inverse Laplace transformation on both sides of Eq. (1), the following formulations for self-excited lift and moment (aeroelastic forces) in time domain can be obtained:

$$L_{se}(t) = \frac{1}{2}\rho U^2 B \begin{bmatrix} ((\underline{A}_0)_{11} + (\underline{F})_{11})\frac{h}{B} + (\underline{A}_1)_{11}\frac{\dot{h}}{U} - (\underline{F})_{11}\frac{\lambda_L U}{B^2}\int_0^t e^{-\frac{U}{B}\lambda_L(t-\tau)}h(\tau)d\tau \\ +((\underline{A}_0)_{12} + (\underline{F})_{12})\alpha + (\underline{A}_1)_{12}\frac{B}{U}\dot{\alpha} - (\underline{F})_{12}\frac{\lambda_L U}{B}\int_0^t e^{-\frac{U}{B}\lambda_L(t-\tau)}\alpha(\tau)d\tau \end{bmatrix} \quad (11)$$

$$M_{se}(t) = \frac{1}{2}\rho U^2 B^2 \begin{bmatrix} ((\underline{A}_0)_{21} + (\underline{F})_{21})\frac{h}{B} + (\underline{A}_1)_{21}\frac{\dot{h}}{U} - (\underline{F})_{21}\frac{\lambda_M U}{B^2}\int_0^t e^{-\frac{U}{B}\lambda_M(t-\tau)}h(\tau)d\tau \\ +((\underline{A}_0)_{22} + (\underline{F})_{22})\alpha + (\underline{A}_1)_{22}\frac{B}{U}\dot{\alpha} - (\underline{F})_{22}\frac{\lambda_M U}{B}\int_0^t e^{-\frac{U}{B}\lambda_M(t-\tau)}\alpha(\tau)d\tau \end{bmatrix} \quad (12)$$

The above formulations can be used to predict self-excited forces and flutter speed in time domain. Aeroelastic self-excited forces can be calculated using Eqs. (11) and (12) at all wind speeds generated in the experiments using the model displacements h and α as recorded, their first derivatives as calculated by finite difference method and the Rational Function Coefficients as extracted. The numerically generated aerodynamic force time histories were compared with those obtained experimentally at wind speeds other than those used in the extraction procedure of Rational Function Coefficients to verify the accuracy of the method. For the streamlined model, comparisons of lift and moment time histories at wind speed of 11.7 m/s are shown in Figs. 7 and 8, respectively. For the bluff model, comparisons of the lift and moment time histories at wind speed of 11.6 m/s are shown in Figs. 9 and 10, respectively. As can be observed in the plots for the streamlined model, both lift and moment time histories matched very well, while the matching is slightly worse for the bluff section model. In the plots for the bluff section model, the amplitudes of predicted lift and moment time histories (by Rational Functions) are slightly

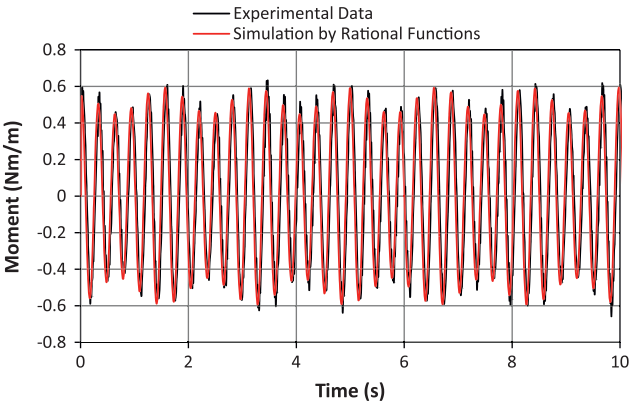

Fig. 8. Moment time histories for the streamlined section model at velocity of 11.7 m/s.

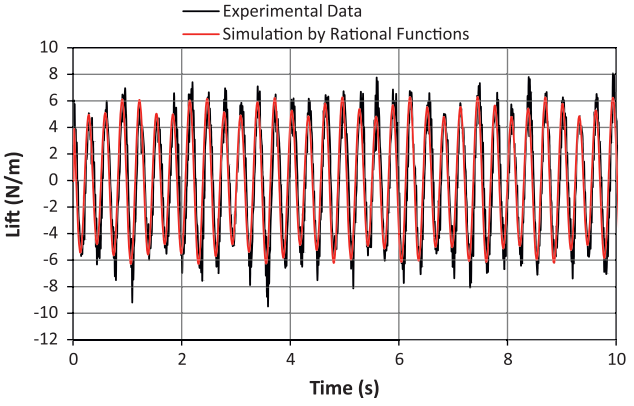

Fig. 9. Lift time histories for the bluff section model at velocity of 11.6 m/s.

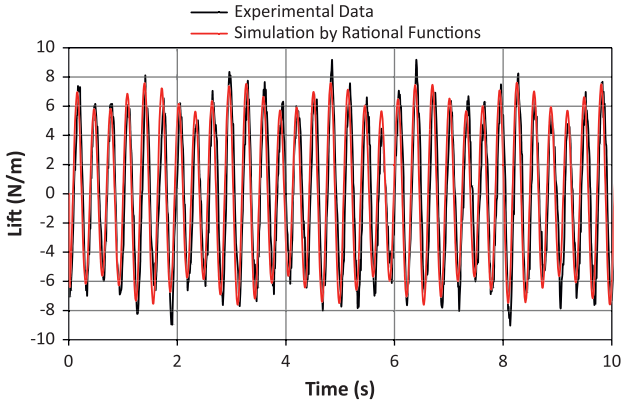

Fig. 7. Lift time histories for the streamlined section model at velocity of 11.7 m/s.

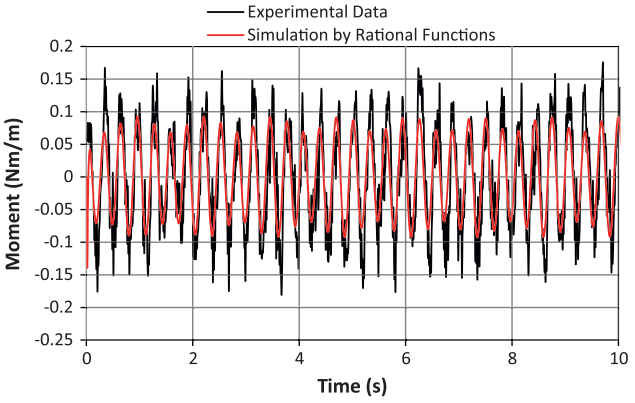

Fig. 10. Moment time histories for the bluff section model at velocity of 11.6 m/s.

Table 2
Parameters for time history comparisons.

	ρ_{xy}	Err_{peak} (%)
Lift (streamlined model)	0.85	1.55
Moment (streamlined model)	0.88	0.40
Lift (bluff model)	0.88	6.96
Moment (bluff model)	0.81	38.22

smaller than those of experimentally measured ones, especially for the lift. To better compare these time histories, cross-correlation coefficient, ρ_{xy}, and percentage peak error, err_{peak}, defined as below were calculated and listed in Table 2.

$$\rho_{xy} = \frac{\frac{1}{n}\sum_{i=1}^{n} x_i y_i}{\sigma_x \sigma_y} \tag{13}$$

$$err_{peak} = \frac{\frac{1}{n}\sum_{i=1}^{n} (\hat{x}_i - \hat{y}_i)^2}{\sqrt{\frac{1}{n}\sum_{i=1}^{n} \hat{x}_i^2}\sqrt{\frac{1}{n}\sum_{i=1}^{n} \hat{y}_i^2}} \times 100\% \tag{14}$$

where x is experimentally obtained time history, y is simulated time history, $\hat{x}_i (i = 1, 2, \ldots)$ are peak values of time history x, and $\hat{y}_i (i = 1, 2, \ldots)$ are peak values of time history y. From Table 2, it is shown that cross-correlation coefficients for all the time histories are close to 1 which means the comparisons of the whole time histories are good, while the coefficients for lift time histories are lower than those for moment time histories, and the coefficients for the bluff section model are lower than those for the streamlined section model. The percentage peak errors for streamlined model time histories are very low, while those for bluff model time histories are much larger, especially for the moment time history. This shows the similar trend as shown in the cross-correlation coefficient results that the comparisons for the streamlined model time histories are better than those for the bluff model time histories. Actually, a similar trend can also be found in earlier flutter derivative studies (e.g., [21]).

For further validation, the flutter speed of the streamlined section model was predicted using time domain simulation and Rational Function Coefficients obtained in this experiment. For flutter speed prediction, the time domain equations of motion were solved at each time step after substituting the Rational Function Coefficients extracted here at a chosen wind speed. This process is repeated for incremental wind speeds until a diverging response is obtained. The flutter speed obtained here was compared with that obtained by Gan Chowdhury and Sarkar [17] on the same model using Rational Functions (free vibration) and flutter derivatives and shown in Table 3. Moreover, to investigate the difference between Rational Function Coefficients extracted from one-DOF and two-DOF forced vibration tests, the flutter speed obtained earlier by Cao and Sarkar [20] from two separate one-DOF forced vibration tests was also included in Table 3. As seen in this table, the comparison is good. Similarly, the flutter speed of the bluff section model was also predicted using Rational Function Coefficients obtained in this paper, and compared with that predicted using flutter derivatives obtained by Matsumoto [19], as shown in Table 4. It can be seen that the flutter speed comparison for bluff section model is good, though slightly worse than the streamlined model case.

Table 3
Comparison of flutter speeds of the streamlined section model obtained by different set of parameters.

Flutter derivatives (free vibration, [17])	Rational Functions (free vibration, [17])	Rational Functions (forced vibration, 1DOF, [20])	Rational Functions (forced vibration, 2DOF, current)
Flutter speed, U_{cr} (m/s)			
32.4	31.8	34.5	32.4

Table 4
Comparison of flutter speeds of the bluff section model obtained by different set of parameters.

Flutter derivatives (forced vibration, 1DOF, [19])	Rational Functions (forced vibration, 2DOF, current)
Flutter speed, U_{cr} (m/s)	
19.5	21.7

6. Conclusion

In this paper, a new algorithm has been developed for direct extraction of all the Rational Function Coefficients for one, two or three-DOF forced vibration wind tunnel tests on a section model. The algorithm does not use phase angle difference between displacement and aeroelastic force time histories in the extraction procedure like in previous methods available in the literature. Thus, the error introduced in all the parameters from error in identification of one parameter, i.e., phase angle difference, is eliminated in this algorithm. Rather this new algorithm uses all the recorded data points to identify the unknown parameters in a least square sense that minimizes the error originating from the noisy signals. The proposed algorithm is more efficient than others since it requires data collected at two wind speeds only to extract the full set of Rational Function Coefficients for a two-DOF system. As part of the validation process, the Rational Functions obtained in this paper were converted into flutter derivatives and were compared with directly extracted ones obtained in earlier experiments by other scholars, for both streamlined and bluff section models. The comparison is well, especially for the streamlined model case. Moreover, it was shown that the Rational Function Coefficients obtained using this algorithm can be used to accurately predict the self-excited forces acting on a section model at a given wind speed, for both a streamlined cross-section and a bluff cross-section. Further, the flutter speed of the streamlined cross-section bridge deck model was predicted using Rational Function Coefficients obtained here and has been shown to match with earlier results. In the future, to validate the application of Rational Functions to predict the response of a bridge deck in a nonstationary wind environment, free vibration tests in a gusty wind (ramp down function applied to mean speed) was performed on a streamlined section model with the same geometry as the model used in this paper but with a larger scale. The results of this validation are quite favorable and will be presented separately.

References

[1] Scanlan RH, Tomko JJ. Airfoil and bridge deckflutter derivatives. J Eng Mech Div 1971;97(6):1717–33.
[2] Scanlan RH. The action of lexible bridges under wind. I: flutter theory. J Sound Vib 1978;60(2):187–99.
[3] Sarkar PP, Jones NP, Scanlan RH. Identification of aeroelastic parameters of flexible bridges. J Eng Mech 1994;120(8):1718–42.
[4] Brownjohn JMW, Jakobsen JB. Strategies for aeroelastic parameter identification from bridge deck free vibration data. J Wind Eng Ind Aerodyn 2001;89:1113–36.
[5] Gan Chowdhury A, Sarkar PP. A new technique for identification of eighteen flutter derivatives using a three-degree-of-freedom section model. Eng Struct 2003;25(14):1763–72.
[6] Lin YK, Ariaratnam ST. Stability of bridge motion in turbulent winds. J Struct Mech 1980;8(1):1–15.
[7] Scanlan RH. Role of indicial functions in buffeting analysis of bridges. J Struct Eng 1984;110(7).

[8] Scanlan RH. Problematics in formulation of wind-force models for bridge decks. J Eng Mech, ASCE 1993;119(7):1353–75.
[9] Chen X, Kareem A. Advances in modeling of aerodynamic forces on bridge decks. J Eng Mech, ASCE 2002;128(11):1193–205.
[10] Caracoglia L, Jones NP. Time domain vs. frequency domain characterization of aeroelastic forces for bridge deck sections. J Wind Eng Ind Aerodyn 2003;91:371–402.
[11] Roger K. Airplane math modeling methods for active control design. AGARD-CP-228; 1977
[12] Karpel M. Design for active flutter suppression and gust alleviation using state-space aeroelastic modeling. J Aircraft 1982;19(3):221–7.
[13] Xie J. CVR method for identification of nonsteady aerodynamic model. J Wind Eng Ind Aerodyn 1988;29:389–97.
[14] Xiang H, Xie J, Lin Z. Aerodynamic study on a proposed cable-stayed bridge in Shanghai, China. J Wind Eng Ind Aerodyn 1988;29:419–27.
[15] Wilde K, Fujino Y, Masukawa J. Time domain modeling of bridge deck flutter. Struct Eng/Earthq Eng, JSCE 1996;13(2):93–104.
[16] Chen X, Matsumoto M, Kareem A. Time domain flutter and buffeting response analysis of bridges. J Eng Mech 2000;126(1):7–16.
[17] Gan Chowdhury A, Sarkar PP. Experimental identification of rational function coefficients for time-domain flutter analysis. Eng Struct 2005;27(9):1349–64.
[18] Haan Jr FL. The effects of turbulence on the aerodynamics of long-span bridges. Dissertation, University of Notre Dame, Notre Dame, Indiana; 2000.
[19] Matsumoto M. Aerodynamic damping of prisms. J Wind Eng Ind Aerodyn 1996;59(2–3):159–75.
[20] Cao B, Sarkar PP. Identification of rational functions by forced vibration method for time-domain analysis of flexible structures. In: Proceedings: the fifth international symposium on computational wind engineering, Chapel Hill; 2010.
[21] Sarkar PP, Caracoglia L, Haan Jr FL, Sato H, Murakoshi J. Comparative and sensitivity study of flutter derivatives of selected bridge deck sections. Part 1: analysis of inter-laboratory experimental data. Eng Struct 2009;31(1):158–69.
[22] Gan Chowdhury A, Sarkar PP. Identification of eighteen flutter derivatives of an airfoil and a bridge deck. Wind Struct 2004;7(3):187–202.
[23] Sarkar PP, Gan Chowdhury A, Gardner TB. A novel elastic suspension system for wind tunnel section model studies. J Wind Eng Ind Aerodyn 2004;92(1):23–40.